Original Article

Circular RNA *SPECC1* promoted tumorigenesis and osimertinib resistance in lung adenocarcinoma via a circular RNA-microRNA network

Zhexue Hao[1#], Fenlan Feng[2#], Qi Wang[2#], Yucong Wang[3], Jin Li[2], Jinkun Huang[4]

[1]Department of Thoracic Surgery, The First Affiliated Hospital of Guangzhou Medical University, Guangzhou, China; [2]The Key Laboratory of Advanced Interdisciplinary Studies, The State Key Laboratory of Respiratory Disease, The First Affiliated Hospital of Guangzhou Medical University, Guangzhou, China; [3]Department of Laboratory Medicine, The First Affiliated Hospital of USTC, The RNA Institute, School of Basic Medical Sciences, Division of Life Science and Medicine, University of Science and Technology of China (USTC), Hefei, China; [4]Department of Urology, Guangdong Provincial Key Laboratory of Urology, The First Affiliated Hospital of Guangzhou Medical University, Guangzhou, China

Contributions: (I) Conception and design: J Li; (II) Administrative support: J Li, J Huang, Z Hao; (III) Provision of study materials or patients: Z Hao, F Feng; (IV) Collection and assembly of data: Q Wang, F Feng, Y Wang; (V) Data analysis and interpretation: Q Wang, F Feng, Y Wang; (VI) Manuscript writing: All authors; (VII) Final approval of manuscript: All authors.

[#]These authors contributed equally to this work.

Correspondence to: Jinkun Huang, PhD. Department of Urology, Guangdong Provincial Key Laboratory of Urology, The First Affiliated Hospital of Guangzhou Medical University, No. 151 Yanjiang West Road, Yuexiu District, Guangzhou 510120, China. Email: HJK@gzhmu.edu.cn.

Background: Tyrosine kinase inhibitors (TKIs) are the first-line therapy for patients with non-small cell lung cancer (NSCLC) with sensitized mutations in the epidermal growth factor receptor (*EGFR*). However, resistance to TKIs is a major clinical issue that affects the survival and prognosis of the patients, with the mechanisms underlying this resistance remaining elusive. Circular RNAs (circRNAs) are a class of single-stranded, covalently closed RNA molecules, which are generated from pre-messenger RNAs (mRNAs) through back splicing. The aim of this study was to investigate the role of cRNA SPECC1 in promoting resistance to TKIs in NSCLC and to explore its potential involvement in tumorigenesis and metastasis of lung adenocarcinoma (LUAD).

Methods: In this study, we identified differentially expressed genes through RNA sequencing from three tumor samples obtained from patients with poor postoperative TKI treatment outcomes. Validation was performed using quantitative real-time polymerase chain reaction (qRT-PCR) and cell function experiments. We further constructed a competing endogenous RNA (ceRNA) network and performed Gene Ontology (GO) analysis to explore the underlying mechanisms of circRNA.

Results: *SPECC1* circular RNA (circ*SPECC1*) was found to be significantly upregulated in tumors as compared to adjacent tissues. Knockdown of circ*SPECC1* in NSCLC cell lines resulted in decreased proliferation, migration, and invasion. Additionally, apoptosis was increased in cell lines with TKI-sensitive *EGFR* mutations when treated with osimertinib.

Conclusions: circ*SPECC1* may promote TKI resistance and contribute to the tumorigenesis and metastasis of NSCLC. This study offers a novel perspective on TKI resistance research at the RNA level.

Keywords: Tyrosine kinase inhibitor resistance (TKI resistance); circular RNA (circRNA); competing endogenous RNA network (ceRNA network); lung adenocarcinoma (LUAD); *SPECC1* circular RNA (circ*SPECC1*)

Submitted Dec 09, 2024. Accepted for publication Dec 23, 2024. Published online Dec 28, 2024.
doi: 10.21037/jtd-2024-2144
View this article at: https://dx.doi.org/10.21037/jtd-2024-2144

Introduction

Among tumors, lung cancer is one of the most malignant, and its morbidity and mortality are increasing, with one-fifth of cancer-related deaths being attributable to this disease (1). Lung adenocarcinoma (LUAD) is one of the most common pathological subtypes of lung cancer, and 30% patients with LUAD harbor the epidermal growth factor receptor (EGFR) mutation, including exon 19 deletion (about 45–50% of *EGFR* mutations) and L858R point mutation in exon 21 (about 40–45% of *EGFR* mutations) (2-5). Activated mutations of *EGFR* are considered to be clinically responsive to tyrosine kinase inhibitors (TKIs) (6-8).

The first-generation TKIs, erlotinib and gefitinib, were developed to target those tumors with *EGFR* mutations. Specifically, they targeted mutations of L858R and exon 19 deletion by reversibly inhibiting the autophosphorylation of EGFR (9). The second-generation TKI, afatinib, could irreversibly inhibit pan-ErbB (10). Although a portion of patients can benefit from disease relief after administration of first- and second-generation TKIs, others experience acquired resistance. Among the patients resistant to gefitinib or erlotinib, 43–50% are positive for T790M mutations (11). Third-generation TKIs, including osimertinib, were designed to target both EGFR sensitizing mutations and T790M resistance mutations (12). The reported progression-free survival of patients treated with osimertinib is 10–12 months (13,14). However, similar to patients treated with first- or second-generation EGFR TKIs, resistance eventually occurs in patients treated with osimertinib. The development of the *EGFR* C797S mutation is one of the most commonly reported mechanisms of resistance to third-generation EGFR TKIs (15). Other EGFR-independent mechanisms of resistance have been reported, such as amplification in MET (16-18), HER-2 (16,19), and FGFR (20); MAPK activation (20); PTEN deletion (21); and transformation to small cell lung cancer (SCLC) (22). Histone lysine demethylases influence cell signaling pathways and promote changes in the tumor microenvironment, leading to resistance to TKIs (23). Osimertinib is a targeted therapy for EGFR mutations in the treatment of non-small cell lung cancer (NSCLC). Although it demonstrates significant efficacy in the early stages of treatment, tumor cells ultimately develop resistance, leading to disease progression. Following osimertinib treatment, tumor cells may alter their growth patterns under drug pressure and potentially influence their interactions with surrounding tissues, thereby contributing to the occurrence of metastasis (24). The clinical characteristics of osimertinib resistance include: imaging studies indicating tumor enlargement or the occurrence of metastasis, tissue biopsies revealing mutations in resistance-related genes (such as C797S) or other molecular markers, blood tests detecting circulating tumor DNA (ctDNA), changes in patient symptoms (such as dyspnea and cough), as well as alterations in patient survival duration (15-22,25). However, the resistance mechanism is complex and still not fully understood.

Circular RNAs (circRNAs) are a class of single-stranded, covalently closed RNA molecules, which are generated from pre-messenger RNAs (mRNAs) through back splicing (26). It was reported that circRNA could sequester microRNA (miRNA) via miRNA response elements (MREs) and serve as miRNA sponges through a competing endogenous RNA (ceRNA) mechanism (27,28). Emerging evidence suggests that the abnormal expression of circRNAs contributes to the tumorigenesis and development of NSCLC as well as its differentiation to drug resistance (29-31). circ_0000567, a circRNA that is differentially expressed in lung cancer before and after gefitinib resistance, was reported to

Highlight box

Key findings

- *SPECC1* circular RNA (circ*SPECC1*) was significantly upregulated in non-small cell lung cancer (NSCLC) tumors as compared to adjacent tissues.
- Knockdown of circ*SPECC1* reduced proliferation, migration, and invasion in NSCLC cell lines.
- Increased apoptosis was observed in tyrosine kinase inhibitor (TKI)-sensitive epidermal growth factor receptor (*EGFR*) mutation cell lines treated with osimertinib.
- Construction of a competing endogenous RNA network and Gene Ontology analysis indicated that circ*SPECC1* promotes TKI resistance.

What is known and what is new?

- TKIs are effective for treating patients with NSCLC and *EGFR* mutations, but resistance is a major issue.
- circ*SPECC1* was found to be involved in TKI resistance, representing a novel insight into resistance mechanisms at the RNA level.

What is the implication, and what should change now?

- Understanding circ*SPECC1*'s role in TKI resistance could lead to the development of new therapeutic targets.
- Future research should focus on developing strategies to counteract *SPECC1*-mediated resistance.

Table 1 Patient characteristics and clinical data

Characteristics	Discovery group, n [%]	Validation group, n [%]
Sample type		
Tumor	3 [50]	20 [50]
Normal	3 [50]	20 [50]
Age (years)		
≤65	1 [33]	10 [50]
>65	2 [67]	10 [50]
Gender		
Female	0 [0]	11 [55]
Male	3 [100]	9 [45]
Smoking status		
Yes	0 [0]	4 [20]
No	3 [100]	16 [80]
Histology		
LUAD	3 [100]	20 [100]
LUSC	0 [0]	0 [0]
Other	0 [0]	0 [0]
Stage		
I	1 [33]	15 [75]
II	1 [33]	1 [5]
IIIA	1 [33]	4 [20]
IIIB	0 [0]	0 [0]
IV	0 [0]	0 [0]
Differentiation		
Well	0 [0]	0 [0]
Moderate	3 [100]	20 [100]
Poor	0 [0]	0 [0]
Tumor nodularity		
Unilateral pulmonary	3 [100]	20 [100]
Bilateral pulmonary	0 [0]	0 [0]
Pleural involvement		
Yes	1 [33]	8 [40]
No	2 [67]	12 [60]
Lymph node involvement		
Yes	1 [33]	6 [30]
No	2 [67]	14 [70]
Vascular invasion		
Yes	0 [0]	14 [70]
No	3 [100]	6 [30]
Postoperative TKI treatment		
Yes	3 [100]	0 [0]
No	0 [0]	0 [0]

LUAD, lung adenocarcinoma; LUSC, lung squamous cell carcinoma TKI, tyrosine kinase inhibitor.

promote the proliferation of gefitinib-resistant cancer cells (32). Moreover, it was found that circ_0048234 may regulate the resistance of EGFR target therapy in colorectal cancer (33-35). However, the circRNAs associated with the third-generation TKIs resistance in NSCLC have not been identified. Therefore, in this study, we attempted to clarify the relationship between circRNAs and resistance to third-generation TKIs in lung cancer. We present this article in accordance with the MDAR reporting checklist (available at https://jtd.amegroups.com/article/view/10.21037/jtd-2024-2144/rc).

Methods

Clinical samples

Tumor samples and adjacent noncancerous samples were obtained from patients with LUAD from The First Affiliated Hospital of Guangzhou Medical University. All tumors and paired nontumor samples were confirmed by experienced pathologists. All samples were rinsed with diethylpyrocarbonate (DEPC)-treated water and then kept in RNAlater (cat. no. AM7020; Invitrogen, Thermo Fisher Scientific, Waltham, MA, USA) for 30 minutes (36,37). We used three paired tumor samples with background tissue from patients with postoperative TKI treatment as the discovery set and 20 paired tumor samples from patients after surgery as the validation set. The detailed clinical features are provided in *Table 1*. The study was conducted in accordance with the Declaration of Helsinki (as revised in 2013). The study was approved by the Ethics Committee of The First Affiliated Hospital of Guangzhou Medical University (Nos. 2018-82 and ES-2024-K161-01) and

written informed consent was taken from all the patients.

Cell culture

Normal lung bronchial epithelium cell line (BEAS-2B) (BEBM) and lung cancer cell lines (PC9, A549, H1975, H1299, H1650, H441) were purchased from the National Collection of Authenticated Cell Cultures (Salisbury, UK). The BEAS-2B cell line was cultured with the base medium for BEBM along with additives (Clonetics Corporation, Lonza, Basel, Switzerland). For lung cancer cell lines, A549 was cultured with Dulbecco's Modified Eagle Medium (DMEM) (cat. no. C11995500B; Gibco, Thermo Fisher Scientific), and all of the other above-mentioned lung cancer cell lines were cultured with RPMI 1640 medium (cat. no. C11875500B; Gibco). All cells were cultured under conditions including 10% fetal bovine serum (FBS) at 37 ℃ in a 5% CO_2 atmosphere.

RNA interference knockdown

We used small interfering RNA (siRNA) (cat. no. A01001; GenePharma, Shanghai, China) to silence the related genes (GenePharma). The sequence of siRNAs targeting human *SPECC1* circular RNA (circ*SPECC1*) were Δcirc*SPECC1* (sense, GUCUGCUGGCCAAGGGGCCT; antisense, GGCCCCUUGGCCAGCAGACTT) and Δcirc*SPECC1*-2 (sense, GCCAAGGGGCCUUUACAACTT; antisense, GUUGUAAAGGCCCCUUGGCTT). The siRNA was transfected into LUAD cells via Lipofectamine 3000 (cat. no. L3000015; Invitrogen) according to the manufacturer's instructions, at least two experiments were repeated.

Cell proliferation and cell cycle assay

Cells were seeded at 1,000 cells per well in 96-well culture plates, and Cell Counting Kit-8 (CCK8) assays were performed with the corresponding kit (cat. no. K1018—5 mL; ApexBio, Houston, TX, USA) following the manufacturer's guidelines. The absorbance value was measured at 450 nm using a Cytation Imaging Reader (BioTek Instruments, Winooski, VT, USA).

For the cell cycle assay, cells were collected, rinsed with phosphate-buffered saline (PBS), and fixed overnight via the addition of absolute ethanol at –20 ℃. Cells were then sequentially washed once in PBS, and cell pellets were resuspended in 0.5 mL of BD Pharmingen Stain Buffer (cat. no. 550825; BD Biosciences, Franklin Lakes, NJ, USA) with propidium iodide (PI) and RNase for 15 minutes at room temperature, and cells were immediately analyzed using the FACSVerse flow cytometer (BD Biosciences), at least two experiments were repeated. The data were analyzed with FlowJo software (FlowJo, LLC, Ashland, OR, USA).

Wound healing assay, invasion assay, and adhesion assay

A wound healing assay was performed when confluence reached 80% to 90%. A wound was created in the center of the cell monolayer by gently removing the attached cells with a pipette tip. A wash with PBS was applied to remove floating cells, and then medium containing 1% FBS was added. Cells were visualized and photographed under an inverted microscope after 24 and 48 hours, at least two experiments were repeated.

For the invasion assay, Transwell chambers were coated on the upper surface with Matrigel Basement Membrane Matrix (10 μg per chamber; cat. no. 356234 Corning Inc., Corning, NY, USA) for at least 2 hours before the experiment. Cells (5×10^4) with pure medium were transferred to the upper chambers of 24-well Transwell chambers (cat. no. 3422; Corning Inc.), with 10% FBS being added to the lower chambers. After 24-hour incubation at 37 ℃, cells in the upper chambers were removed for cell fixation with 4% paraformaldehyde (PFA) and staining with 0.5% crystal violet solution, at least two experiments were repeated.

For the adhesion assay, 5 μg of Matrigel was added in 100 μL of serum-free medium to wells of a 96-well plate and dried in an oven to form an artificial basement membrane. Subsequently, 4.5×10^4 cells were seeded onto the Matrigel basement membrane in 200 μL of normal medium and incubated for 40 minutes. Following incubation, the medium was removed and the membrane washed five times with 150 μL of PBS to remove loosely attached cells. Adherent cells were then fixed in 4% PFA for 15 minutes, and stained in 5% crystal violet solution, at least two experiments were repeated.

EdU staining

The proliferation of cells was determined with BeyoClickTM EdU Cell Proliferation Kit (cat. no. C0078S Beyotime, Nantong, China) according to the manufacturer's protocols. Proliferating cells were washed with PBS twice and incubated with EdU working solution (10 μM) for 2 hours at 37 ℃. Next, the cells were permeabilized with

Table 2 Sequences of primers

Name	Primer sequence 5'-3'
ACTB	F: ACGTTGCTATCCAGGCTGTG
	R: GAGGGCATACCCCTCGTAGA
GAPDH	F: GTCTCCTCTGACTTCAACAGCG
	R: GTCTCCTCTGACTTCAACAGCG
circGLIS2	F: TCAGCCTGTCACCACCATCT
	R: GGAGTTGGAGGTGGCAGCAG
circACVR2A	F: TGCCACTTATGTTAATTGCG
	R: TTCAACACCAGTTTGATTGG
circEPB41L2	F: AAAGCAGAGAAGGCATCTCA
	R: TGGCTAGAGTCCTTCTTCAC
circTET2	F: AGAGTCACCTTCCAAATTAC
	R: GTTCTATCCTGTTCCATCAG
circSPECC1	F: CTGTCTTGCAATGAGCTCAG
	R: CTCTCTTGAGACAGTTACTG
circZKSCAN1	F: ATCCAGTTCAGGAGTCCTCG
	R: CAAACAGGGTCTGTGCTCAC

ACTB, beta-actin; F, forward primer; R, reverse primer; GAPDH, glyceraldehyde-3-phosphate dehydrogenase.

0.1% Triton-X100 for 15 minutes. Following this, the cells were incubated with Click Additive Solution for 30 minutes and 4',6-diamidino-2-phenylindole (DAPI) (cat. no. C1005; Beyotime) for 5 minutes in the dark, at least two experiments were performed multiple times. The images were captured with an Olympus IX73 microscope (Olympus, Tokyo, Japan).

Flow cytometry of cell apoptosis

H1975 and PC9 cells were cultured in six-well plates. After 24 hours of transfection, 0.24 μmol/L of osimertinib was added to cells. Subsequently, the cells were collected and stained with an Annexin V-fluorescein 5-isothiocyanate (FITC) apoptosis detection kit (cat. no. 556547; BD Biosciences) and were analyzed with a BD FACSVerse flow cytometer (BD Biosciences) according to the manufacturer's protocol, at least two experiments were repeated.

Hoechst 33342/PI staining assay

H1975 and PC9 cells were cultured in six-well plates. After 24 hours of transfection, 0.24 μmol/L of osimertinib was added to cells. After this, the cells were fixed with 4% polyoxymethylene, washed three times with PBS, and incubated in PBS with 5 μL of Hoechst33342 and 5 μL of PI (cat. no. C0003; Beyotime) for 30 minutes at 4 ℃. Cells were washed twice with PBS and observed using an Olympus IX73 fluorescence microscope (Olympus). ImageJ software (National Institutes of Health, Bethesda, MD, USA) was used to analyze the results.

Total RNA extraction

The clinical samples were dissected into small fragments and subsequently homogenized in TRIzol reagent (cat. no. 15596018CN; Invitrogen) with a homogenizer to ensure thorough lysis of cellular components (CCs). Total RNA was extracted via using TRIzol reagent according to the manufacturer's instructions, including phase separation with chloroform, RNA precipitation with isopropanol, and washing with ethanol to obtain purified RNA. The quality and quantity of the extracted RNA were assessed using a spectrophotometer.

Reverse transcription and quantitative real-time polymerase chain reaction (qRT-PCR)

RNA was converted to complement DNA (cDNA) via a PrimeScript RT Reagent Kit (cat. no. RR037A; Takara Bio, Kusatsu, Japan) according to the manufacturer's instructions. qRT-PCR was performed with KAPA SYBR FAST qPCR Master Mix (cat. no. KK4601; KAPA Biosystems, Wilmington, MA, USA) on a CFX96 Real-Time PCR System (Bio-Rad Laboratories, Hercules, CA, USA) according to standard procedures. The levels of circRNAs were normalized to the levels of beta-actin (*ACTB*) or glyceraldehyde-3-phosphate dehydrogenase (*GAPDH*). The results of qRT-PCR were evaluated, expressed as the cycle threshold (Ct) value, converted into fold change (FC), and each sample is generally subjected to three technical replicates. PCR was performed with Premix Taq (Takara Bio). All the primers are shown in *Table 2*.

The library construction and high-throughput sequencing

Total RNA from three pairs of LUAD patients was extracted for high-throughput sequencing. Total RNA (10 μg) was used to construct the whole transcriptome library with the TruSeq Ribo Profile Library Prep Kit (Illumina, San Diego, CA, USA) according to the

manufacturer's instructions. In brief, ribosomal RNA was depleted with the Ribo-Zero Gold Kit (Illumina), and surplus RNA was purified for end repair and 50-adaptor ligation. Following this, reverse transcription was performed with random primers containing 3' adaptor sequences. Finally, the cDNAs were purified and amplified with PCR reactions. The products in 300–500 lengths were purified and quantified. These libraries were used for 150-nt paired-end sequencing with an HiSeq PE150 system (Illumina). Each library has generated at a depth of ~50 million read pairs, and then adapters sequences were removed using Cutadapt to obtain clean read. For small RNA (sRNA), six sRNA libraries were generated with TruSeq small RNA (Illumina), according to the manufacturer's instructions. The prepared libraries were used for 50-nt single-end sequencing with a HiSeq SE150 system (Illumina). Any reads shorter than 15-nt were filtered out to obtain clean reads. Our sequencing data has been deposited in a public repository (http://www.ncbi.nlm.nih.gov/bioproject/707622).

Transcriptome sequencing data analysis

The high-throughput sequencing tools, Hisat2 (38), Samtools (39), and feature counts (40) were used to map clean reads to the *Homo sapiens* reference genome (hg19) and to calculate the gene expression level, which was normalized to the z score. To determine the differentially expressed mRNAs, the "DEseq2" package in R software (The R Foundation of Statistical Computing) was used with the corresponding cutoff (q <0.05 and |log2 FC| >1 for mRNA). To predict the circRNAs, we identified the possible candidates with find_circ (41), and the junction reads were normalized to z score. The criteria of P<0.05 and |log2 FC| >1 were used to identify differentially expressed circRNAs in the three pairs of samples. The Cancer-Specific CircRNA database (CSCD; http://gb.whu.edu.cn/CSCD/) was referenced for the prediction of MRE and RNA binding protein (RBP) among the differentially expressed circRNAs. For sRNA, the clean reads were mapped to the human genome (hg19) and the miRNA database in miRBase with bowtie (-v 1). The differentially expressed miRNAs were determined via the R package "DEseq2" according to the cutoffs of P<0.05 and |log2 FC| >1.

Construction of the ceRNA network

For the ceRNA network of significantly dysregulated circRNAs, mRNAs, and miRNAs, the miRNA-mRNA and miRNA-circRNA interactions were determined according to a correlation coefficient parameter of an R^2 value >0.99. These networks were constructed using Cytoscape (https://cytoscape.org/).

Gene Ontology (GO) analysis

GO enrichment analysis of the target genes in the networks was performed with the "cluster profiler" package in R. GO analysis included three aspects—CCs, molecular functions (MFs), and biological processes (BPs)—and was conducted according to previously reported methods (42,43).

Survival analysis

The University of ALabama at Birmingham CANcer data analysis Portal (UALCAN) online tool (http://ualcan.path.uab.edu) was used to analyze the significantly dysregulated mRNAs under default parameters.

Statistical analysis

Statistical significance was assessed using the *t*-test. All statistical analyses were performed using SPSS 25 (IBM Corp., Armonk, NY, USA). The values reported in the graphs in this article represent the averages of the actual number of independent experiments, with the error bars indicating the standard deviation (SD).

Results

Identification of differentially expressed circRNAs in LUAD samples

To identify LUAD-associated RNA, RNA sequencing was performed from tumor samples and paired adjacent nontumor samples from three patients with LUAD. Subsequently, the differential expression analysis of mRNAs, circRNAs, and miRNAs was performed (Figure S1A). Pearson correlation coefficient analysis demonstrated a significant correlation between tumor samples or normal samples between groups (Figure S1B). The genetic expression of these three pairs of tumor samples was markedly different from that of normal samples, and samples between each group had a high degree of similarity in a principal component analysis (PCA) model (Figure S1C).

We found that the expression level of overall circRNAs in tumor samples was lower than that of the background according to the box diagram (*Figure 1A*). The cumulative distribution function (CDF) showed a faster accumulation of genes in tumor samples (*Figure 1B*). Moreover, the number of circRNA reads with a larger spliced sequence length was relatively higher in tumor samples, which appeared to contain more circRNAs longer than 3,000 nucleotides compared to normal samples (*Figure 1C*,*1D*). Moreover, the differentially expressed circRNAs were identified, and the expression levels of these circRNAs were examined. Through volcano plot and hierarchical cluster analysis, six differentially expressed circRNAs were identified (*Figure 1E*,*1F*), with circGLIS2, circACVR2A, and circEPB41L2 being downregulated in tumor samples and circTET2, circSPECC1, and circZKSCAN1 being upregulated (*Figure 1E*,*1F*).

The open reading frame (ORF) of the six differentially expressed circRNAs was predicted for a potentially translatable template, MRE for potential miRNA binding capabilities, and RBP for circRNA-RBP interactions. As shown in *Figure 1G*, all six of these six circRNAs had MREs, which indicated that they could bind directly to the corresponding miRNAs to inhibit miRNA activity and thus regulate the expression of target genes. Except for circGLIS2, all had predicted RBP binding sites, suggesting that they might function as protein scaffolds. circGLIS2, circEPB41L2, circTET2 and circZKSCAN1 were found to have ORFs, indicating that they might be translated into peptides. Interestingly, circTET2 harbored predominantly ORFs and RBPs, rather than MREs, while circSPECC1 predominantly harbored MREs. The expression level of circRNAs was verified in the LUAD patient cohorts via qRT-PCR. circGLIS2 was significantly downregulated in tumors as compared to background tissues, while circSPECC1 was upregulated in tumors (*Figure 1H*). The expression profile of circRNAs was also screened in a panel of normal bronchial epithelium and LUAD cell lines. The results showed that circGLIS2 was weakly expressed in the A549, H1975, H1299, H1650, and H441 cell lines, while it was highly expressed in the BEAS-2B cell lines. circSPECC1 was highly expressed in BEAS-2B, A549, H1975, H1650, and H441 cell lines, while it was weakly expressed in H1299 cell lines (*Figure 1I*). Therefore, we selected circSPECC1 from six differentially expressed circRNAs for the subsequent experiments.

circSPECC1 promoted tumorigenesis and metastasis in NSCLC cells

To investigate the potential function of circSPECC1 in lung cancer cells, we selected two NSCLC cell lines, H1975 (T790M/L858R) and PC9 (exon 19 deletion), which have been commonly used in previous LUAD studies (44,45). Two rationally designed siRNA oligonucleotides, targeting the back splice junction of circ*SPECC1*, were transfected into cell lines, and the most efficient siRNA was then selected for further investigation (*Figure 2A* and Figure S1D). This siRNA, as shown in *Figure 2A* (Δcirc*SPECC1*), successfully knocked down circ*SPECC1* (~20% reduction; $P<0.05$) but had no effect on the linear *SPECC1* mRNA expression level in H1975 (T790M/L858R) or PC9 (exon 19 deletion) cell lines. A 20%-decrease of Edu-555 fluorescence intensity in these cell lines caused by circ*SPECC1* knockdown indicated that circ*SPECC1* promoted NSCLC cell proliferation (*Figure 2B*,*2C*). The wound healing assay demonstrated that the motility of H1975 and PC9 was inhibited by circ*SPECC1* knockdown. The number of invading NSCLC cells was significantly decreased after circSPECC1 knockdown (*Figure 2D*,*2E*) as was the adhesion ability of H1975 and PC9 cells (*Figure 2F*). In addition, cell cycle analysis further indicated the regulation of circ*SPECC1* in tumor cell proliferation, as shown in Figure S1E, which was associated with a decrease in G2/M and S arrest. Overall, these findings indicate that circ*SPECC*1 could promote the tumorigenesis and metastasis of two NSCLC cell lines and affect the cell cycle.

circSPECC1 reduced the sensitivity of tumor cells to osimertinib

To further determine whether circ*SPECC1* was associated with the sensitivity and resistance to TKI treatment, a CCK8 assay was performed. It was found that the proliferation of H1975 and PC9 cells decreased after 72 hours of circ*SPECC1* knockdown. Under osimertinib treatment, cell proliferation was further inhibited, and the original sensitivity of H1975 and PC9 cells to TKIs was restored (*Figure 3A*,*3B*). Notably, with a 24-hour treatment of osimertinib, the number of apoptotic cells increased significantly in Δcirc*SPECC1* H1975 cells and Δcirc*SPECC1* PC9 cells as compared to control cells (*Figure 3C*,*3D*). As can be seen in *Figure 3E*,*3F*, Hoechst 33342 and PI assay

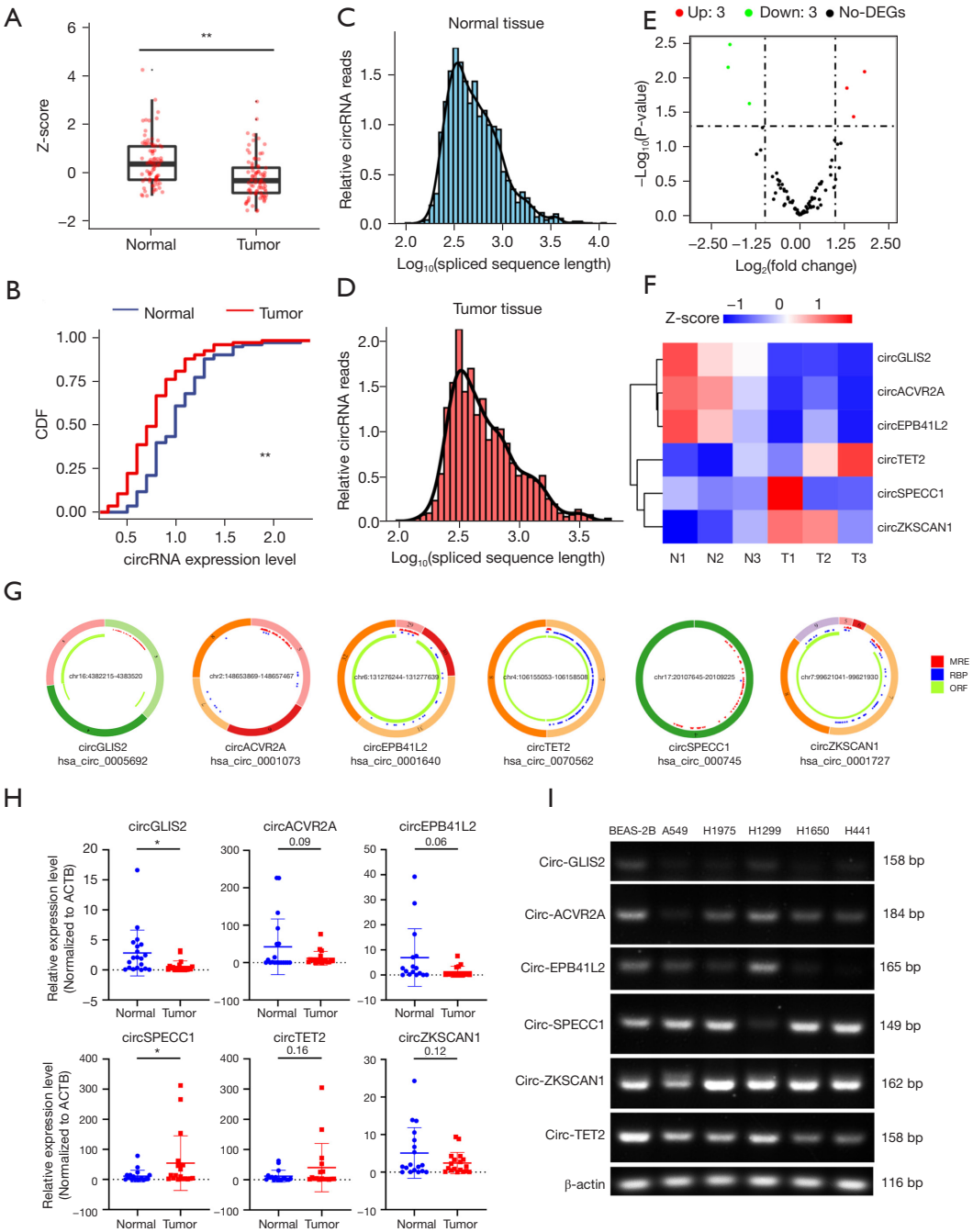

Figure 1 Identification of dysregulated circRNAs from RNA-seq. (A) Boxplot of all circRNA expression levels in normal and tumor tissue, respectively. (B) The cumulative distribution function for LUAD circRNA expression in normal and tumor tissue, respectively. (C,D) The distribution of circRNA spliced sequence length among normal and LUAD tissues. (E) Volcano plot of the differentially expressed circRNAs. (F) Heatmap of the expression level of differentially expressed circRNAs. (G) Detailed information and element prediction for six differentially expressed circRNAs. (H) The validation results of 6 dysregulated circRNAs from qRT-PCR. (I) Expression profile of 6 dysregulated circRNAs from a PCR assay. Data are the mean ± SD. P<0.05 for the *t*-test. *, P<0.05; **, P<0.01. circRNA, circular RNA; CDF, cumulative distribution function; DEGs, differentially expressed genes; MRE, miRNA response element; RBP, RNA binding protein; ORF, open reading frame; ACTB, beta-actin; LUAD, lung adenocarcinoma; qRT-PCR, quantitative real-time polymerase chain reaction; PCR, polymerase chain reaction; SD, standard deviation.

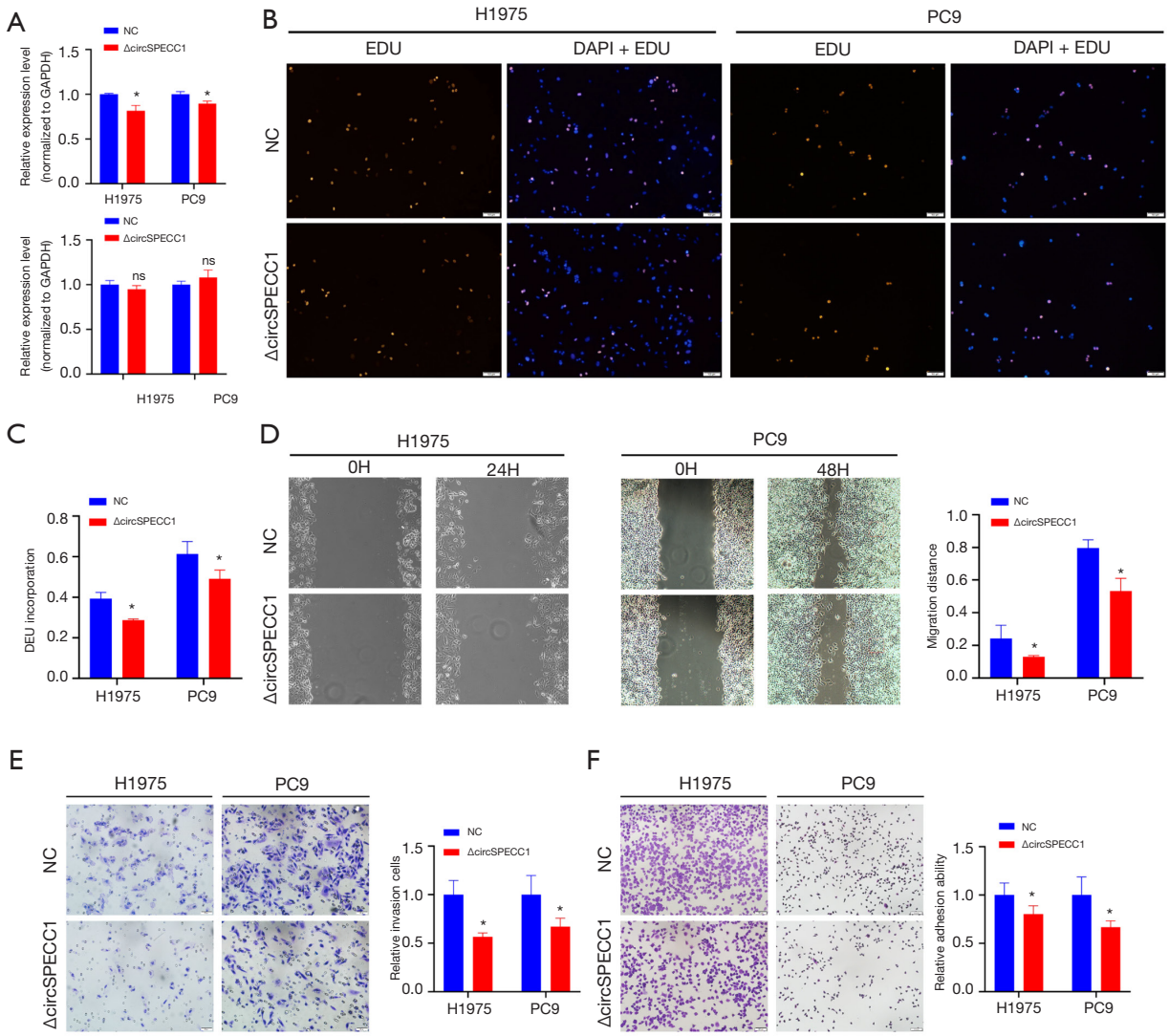

Figure 2 circ*SPECC1* promoted tumorigenesis and metastasis in NSCLC. (A) qRT-PCR detection of circ*SPECC1* after siRNA interference as compared to NCs. (B,C) EdU staining assay showed proliferation of tumor cells after Δcirc*SPECC1* for 24 hours, captured at ×10 magnification. (D) The migration of cells was assessed by wound healing assay, captured at ×20 magnification. (E) The invasion of cells was assessed by Transwell assay with Matrigel, stained by crystal violet, captured at ×20 magnification. (F) The metastasis of cells was assessed by adhesion assay, stained by crystal violet, captured at ×20 magnification. Data are the mean ± SD. P<0.05 for the *t*-test. ns, no significance; *, P<0.05. NC, negative control; *GAPDH*, glyceraldehyde-3-phosphate dehydrogenase; circ*SPECC1*, *SPECC1* circular RNA; NSCLC, non-small cell lung cancer; qRT-PCR, quantitative real-time polymerase chain reaction; siRNA, small interfering RNA; SD, standard deviation.

consistently showed that in the 24 hours of osimertinib treatment, the death rate of cells rose significantly after circ*SPECC1* knockdown as compared to that observed in cells without osimertinib treatment. There was no significant difference in the increase in apoptosis of tumor cells upon circ*SPECC1* knockdown, while with the addition of osimertinib treatment, the increase in apoptosis rate of tumor cells in the knockdown group was twice as high as that in the control group. circ*SPECC1* demonstrated a protective effect against the cell apoptosis induced by osimertinib, which is related to the sensitivity and response of LUAD cells to TKIs.

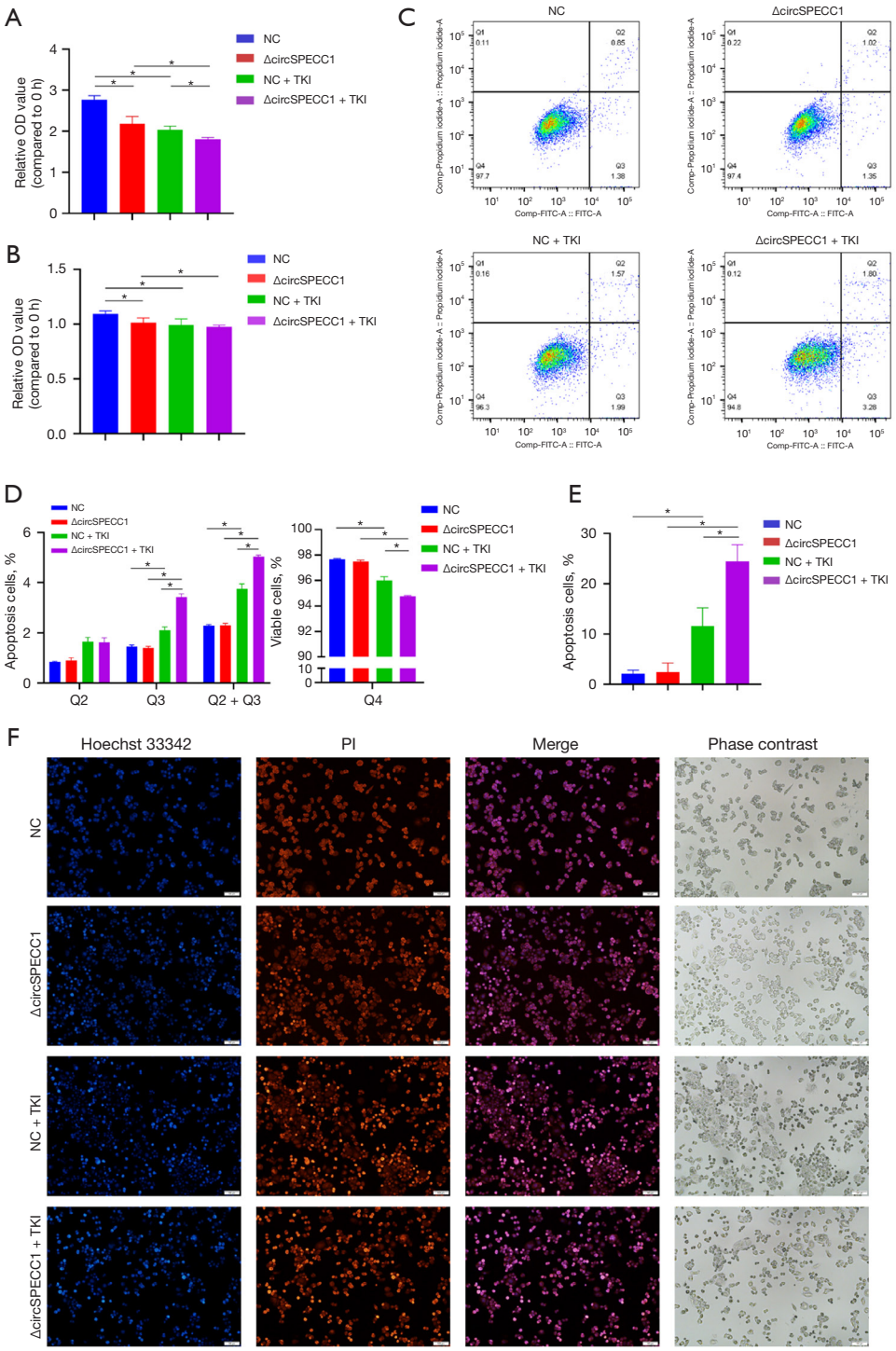

Figure 3 circ*SPECC1* reduced the sensitivity of tumor cells to TKI. (A) Relative OD in H1975 cells after RNA interference and TKI treatment for 72 hours. (B) Relative OD in PC9 cells after RNA interference and TKI treatment for 72 hours. (C,D) Flow cytometry of cell apoptosis after RNA interference and TKI treatment for 24 hours in PC9 cells. (E,F) The rate of cell death was assessed via Hoechst 33342/PI staining assay in PC9 cells after RNA interference and TKI treatment for 24 hours, captured at ×10 magnification. Data are the mean ± SD. P<0.05 for the *t*-test. *, P<0.05. NC, negative control; circ*SPECC1*, *SPECC1* circular RNA; TKI, tyrosine kinase inhibitor; OD, optical density; FITC, fluorescein isothiocyanate; PI, propidium iodide; SD, standard deviation.

Identification of target genes of circRNAs

To identify potential target genes of circRNAs, we aimed to analyze the differentially expressed mRNAs from RNA-sequencing data in the above-mentioned LUAD samples, with 4,137 differentially expressed mRNAs ultimately being screened (*Figure 4A*). Among these, 2,496 (60.33%) were upregulated compared to normal samples, while 1,641 (39.67%) were downregulated (*Figure 4A*). Hierarchical cluster analysis was also performed to evaluate these mRNAs (*Figure 4B*). GO enrichment analysis was performed with three categories: BP, CC, and MF. The top 15 GO terms in terms of enrichment are listed in *Figure 4C*. Cell adhesion molecule binding, collagen-containing extracellular matrix, and extracellular structure organization were the most enriched, indicating that these differentially expressed mRNAs may be closely associated with molecular binding and extracellular matrix organization, which may be associated with tumorigenesis and metastasis. For survival analysis, the UALCAN online tool was used to investigate the relationship between the identified target genes and clinical observations (*Figure 4D*). The top 10 differentially expressed mRNAs were selected according to P value for survival curves analysis, with eight mRNAs being significantly correlated with LUAD patient survival. Among these, six (*LAMA3*, *HMGA1*, *SLC2A1*, *PROM2*, *KRT80*, and *SFN*) were negatively correlated with survival curves (patients with higher expression had shorter survival). Meanwhile, *MFAP4* and *PREX2* were positively correlated with LUAD patient survival (patients with higher expression had longer survival).

Construction of the ceRNA regulatory network

CircRNAs functioning as miRNA sponges have been widely reported in a study (46). As previously demonstrated, circ*SPECC1* has an abundance of MREs but a lack of oligonucleotide repeat domains (ORDs). We screened out dysregulated miRNAs through volcano plot (*Figure 5A*) and constructed a ceRNA network containing differentially expressed circRNAs, miRNAs, and mRNAs to clarify the underlying mechanism of circRNAs' effect in LUAD (*Figure 5B*). In this ceRNA network, 28 miRNAs and 55 mRNAs were found to have correlations with 6 circRNAs. circ*SPECC1* was found to sponge four miRNAs; among these, miR-598-3p, miR-33a-3p, and miR-497-5p were downregulated in clinical samples, while miR-369-3p was upregulated. These miRNAs further affected mRNAs, including *TUBB1*, *BCHE*, *BNIP3*, *LHFPL6*, and *SLC39A4*. We also conducted GO analysis to determine the enrichment of RNA processes, which showed that chromosomal region, cell adhesion molecule binding, extracellular structure organization, and ribosome biogenesis were the most enriched (*Figure 5C*).

Discussion

There is a growing body research suggesting that circRNAs play crucial roles in drug resistance (5,47). We performed high-throughput sequencing on three tumors from patients with poor postoperative TKI treatment outcomes and compared them with paired background tissue. Six circRNAs (circ*SPECC1*, circ*GLIS2*, circ*ACVR2A*, circ*EPB41L2*, circ*TET2*, and circ*ZKSCAN1*) were screened according to z scores in a discovery set of tissue samples associated with poor prognosis after osimertinib treatment. In addition, we noted that there were several circRNA expression profiles (GSE158695, GSE112214, GSE101586, and GSE101684) from lung cancer tissues in the Gene Expression Omnibus (GEO) database (48-51). We therefore examined the expression of the six circRNAs we identified in these data and found that five of them (circ*SPECC1*, circ*TET2*, circ*ACVR2A*, circ*GLIS2*, and circ*EPB41L2*) were included, among which circ*SPECC1* and circ*TET2* were upregulated in tumors, while circ*ACVR2A*, circ*GLIS2*, and circ*EPB41L2* were downregulated; this was consistent with our differentially expressed gene screening and validation results (Figure S2). In the lung cancer cell lines from GSE152434 dataset, circ*SPECC1* and circ*TET2* were highly expressed in A549 cells, while circ*ACVR2A*, circ*GLIS2*, and circ*EPB41L2* were highly expressed in BEAS-2B cells (52).

Interestingly, circ*SPECC1* was found to be markedly upregulated in tumor samples, a finding which was further validated in our study (53-55). circ*SPECC1* was reported to promote hepatocellular and gastric carcinoma tumorigenesis via a ceRNA mechanism (29,30). However, whether circ*SPECC1* is involved in TKI resistance has not been extensively examined. We further investigated the biological function of circ*SPECC1* and its effect on the response of TKIs in NSCLC. First, we found that the proliferation, migration, and invasion ability of NSCLC cell lines were significantly decreased upon circ*SPECC1* knockdown. Second, the apoptotic rate of cell lines with TKI-sensitive EGFR mutation was increased after circ*SPECC1* was knocked down in the presence of osimertinib. Therefore, we hypothesize that circ*SPECC1* may reduce the sensitivity of

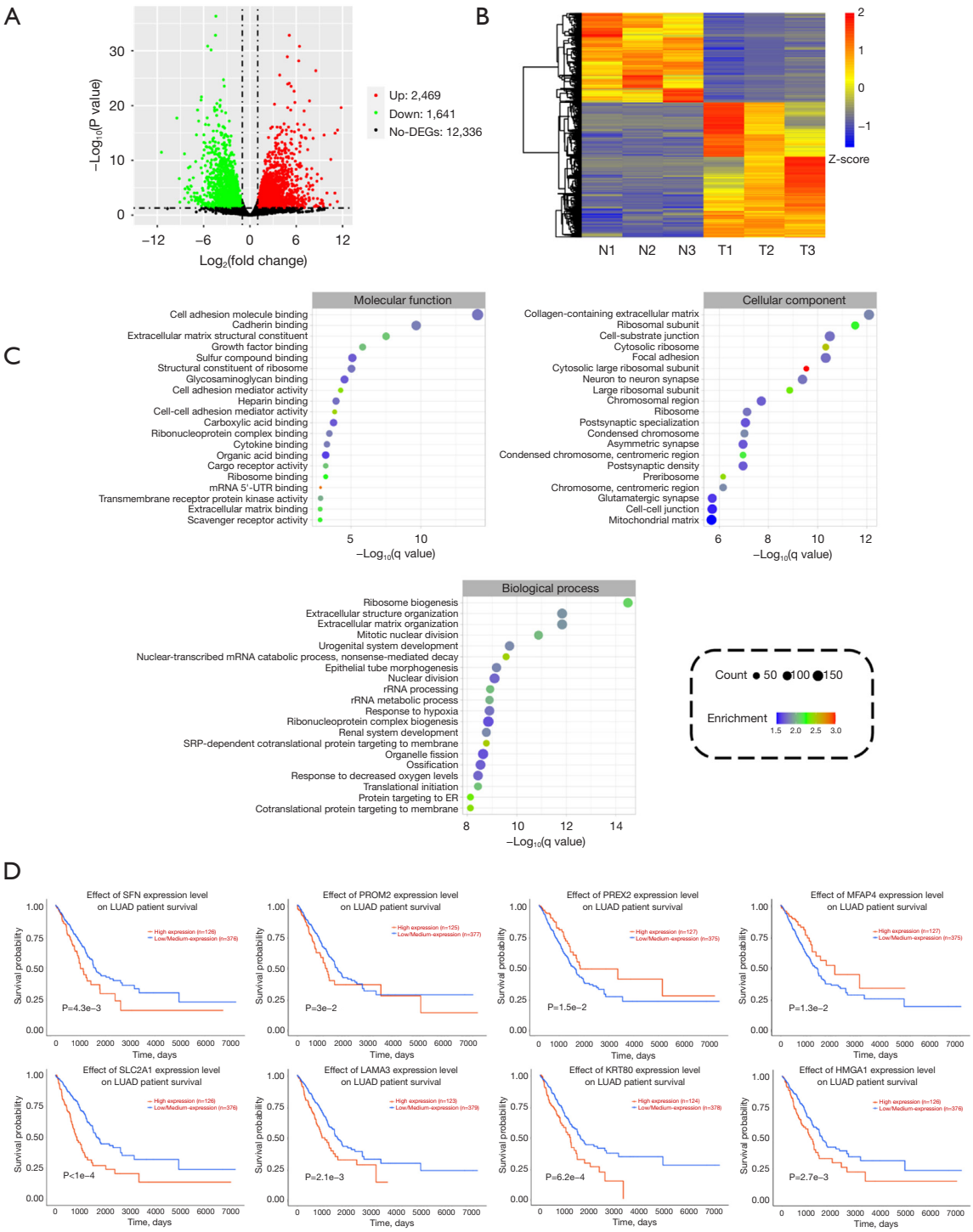

Figure 4 Identification of target genes of circRNAs. (A,B) Volcano plot of the differentially expressed transcripts and the hierarchical cluster heatmap of the differential expression of mRNAs in three LUAD tumor samples and their controls. (C) GO analyses and annotation of dysregulated genes in three main categories: biological processes, cellular components, and molecular functions. (D) Survival curves of identified genes were analyzed by UALCAN analysis. The P value was calculated with the log-rank test. DEGs, differentially expressed genes; mRNA, messenger RNA; UTR, untranslated regions; ER, endoplasmic reticulum; LUAD, lung adenocarcinoma; circRNA, circular RNA; GO, Gene Ontology; UALCAN, University of ALabama at Birmingham CANcer data analysis Portal.

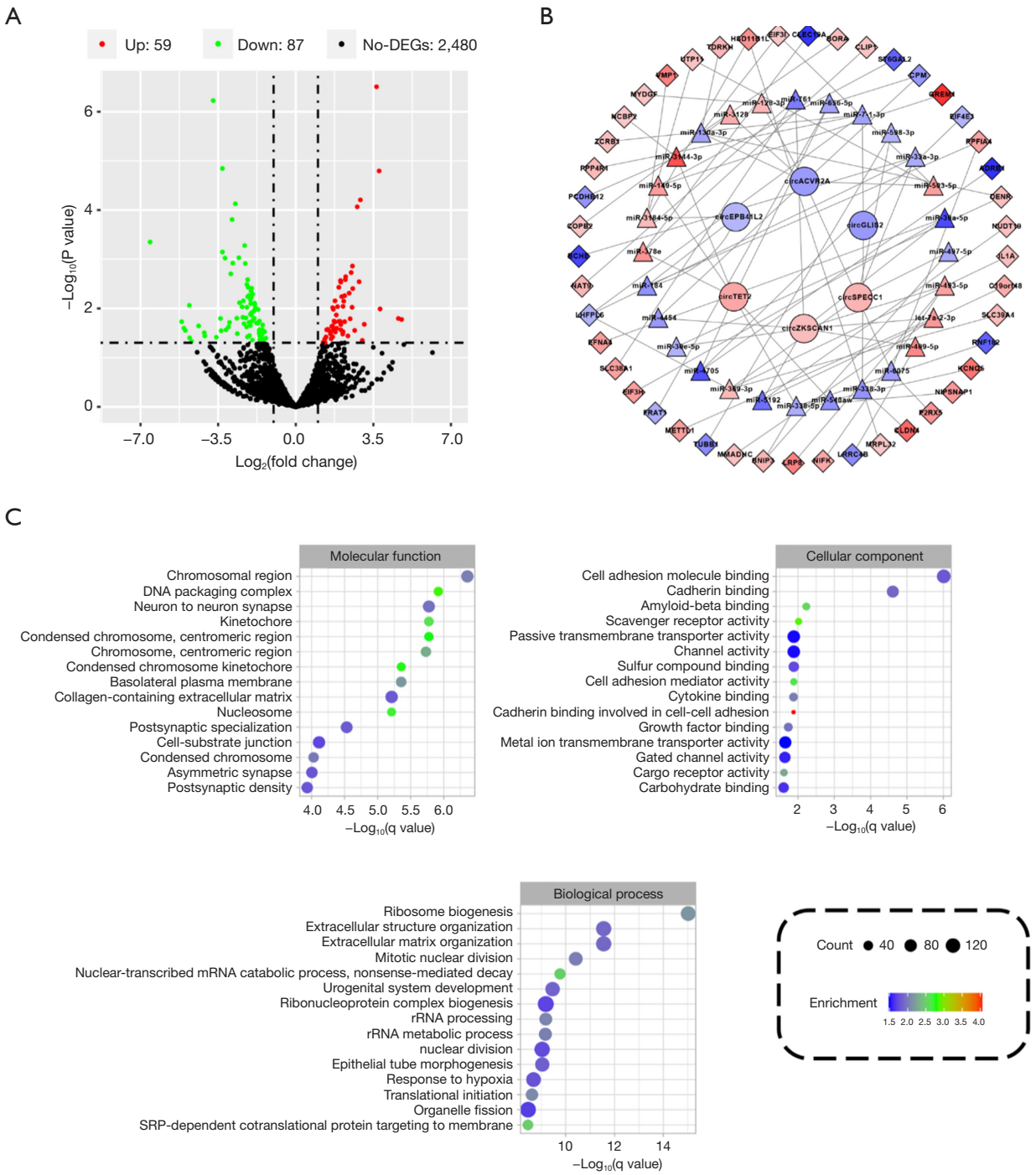

Figure 5 Construction of the competing endogenous RNA regulatory network. (A) Volcano plot of the differentially expressed miRNAs. (B) A ceRNA network was constructed according to the interactions among circRNAs, miRNAs, and mRNAs (correlation coefficient absolute value 0.99). Boxes represent the dysregulated mRNAs, triangles represent the dysregulated miRNAs, and circles represent the dysregulated circRNAs. Red, upregulated; blue, downregulated. (C) GO analyses of the affected pathways in three main categories: cellular components, biological processes, and molecular functions. DEGs, differentially expressed genes; mRNA, messenger RNA; SRP, study reference population; miRNA, microRNA; ceRNA, competing endogenous RNA; circRNA, circular RNA; GO, Gene Ontology.

TKI treatment by targeting *EGFR*-mutant cells, specifically H1975 (T790M/L858R) and PC9 (exon 19 deletion) cells. To characterize the mechanisms underlying the effect of circRNAs on TKI resistance, we further constructed a ceRNA network and performed GO analysis.

We constructed circRNA-miRNA-mRNA networks for circ*SPECC1* and for five other circRNAs. We further screened a group of mRNAs as potential target genes via RNA-sequencing analysis and qRT-PCR. Some of these differentially expressed genes have already been reported to be related to drug resistance in other cancers (56-60). In this network, circ*SPECC1* was predicted to interact with four miRNAs capable of regulating five mRNAs. *TUBB1* has been implicated in the accumulation of DNA damage, which can result in genome instability (61). This process may arise from the most primitive TKI-refractory cells present in both TKI-naive and TKI-treated patients (62). Our GO analysis revealed the pathways these five genes might participate in. The target genes were significantly enriched in the chromosomal region and DNA packaging complex, which may be related to TKI resistance (63). BNIP3-related autophagy caused by gemcitabine leads to reduced lung cancer cell death, which may contribute to gemcitabine-acquired resistance (64). The pathways identified in or GO analysis were mainly related to ribosome biogenesis, mitotic nuclear division, and mRNA catabolic process, which may be related to cell proliferation.

Acquired resistance to EGFR-TKIs has been thought to represent the end product of two different but possibly concurrent evolutionary pathways, including the selection of cancer clones that contain preexisting resistance mutations and the reacquisition of these genetic defects due to random mutations (56). The mechanism of TKI resistance is complex, and its molecular mechanism has only begun to be clarified in recent years. The common resistance mutations of the new the third-generation EGFR-TKIs include L718Q (57), L844V (58), and C797S (58), all of which confer resistance to rociletinib, with C797S conferring resistance to osimertinib (61). The combination of traditional TKIs combined with chemotherapy or other targeted drugs provide a degree of benefit to patients with TKI resistance (65). With the development of the fourth-generation EGFR-TKIs (66), it is necessary to further investigate the mechanisms of drug resistance. At present, there is still a lack of broad-spectrum and inexpensive genetic testing methods in clinical practice. The reason we designed only two siRNAs in this study is that siRNAs targeting circ*SPECC1* must be specifically designed at the splicing junction, thus limiting our choice for circ*SPECC1*-specific siRNAs. One of the siRNAs targeting circ*SPECC1* showed stable knockdown efficiency as high as 20%. CircRNA has the potential to serve as a biomarker for early cancer diagnosis and prognosis assessment, and it may also emerge as a novel therapeutic target to enhance cancer treatment outcomes through interventions in its expression or function. However, despite the significant promise of circRNA in cancer research, several challenges persist. Currently, the methods for detecting and analyzing circRNA are not standardized, which affects the comparability of results. Additionally, the diversity and complex functional mechanisms of circRNA present difficulties in research. Furthermore, the effective translation of circRNA research findings into clinical applications remains to be addressed (67). Therefore, future research should focus on further elucidating the functions and mechanisms through which circRNAs influence TKI resistance, as well as advancing clinical detection methods. Enhancing early detection of TKI resistance is essential for guiding personalized treatment strategies in clinical practice.

Conclusions

We found that circ*SPECC1* participates in the tumorigenesis and TKI resistance of NSCLC and may thus be a candidate for the targeted therapy of NSCLC.

Acknowledgments

We would like to thank the following institutions for providing valuable resources: the State Key Laboratory of Respiratory Disease, the National Clinical Research Center for Respiratory Disease, The First Affiliated Hospital of Guangzhou Medical University, and the School of Basic Medical Sciences, Division of Life Science and Medicine, USTC. We also appreciate the great support from Professor Chen Liang in improving the quality of this paper.

Funding: This study was supported by the project of National Natural Science Foundation of China (No. 82273450), the Project of Guangdong Medical Research Foundation (No. B2021313), the Science and Technology Innovation Committee Joint Funding (Dengfeng Hospital) Project of Guangzhou (Nos. 2023A03J0355, 2023A03J0343 and 2023A03J0356), and the Opening Foundation of the State Key Laboratory of Respiratory Diseases (No. SKLRD-OP-202404).

Footnote

Reporting Checklist: The authors have completed the MDAR reporting checklist. Available at https://jtd.amegroups.com/article/view/10.21037/jtd-2024-2144/rc

Data Sharing Statement: Available at https://jtd.amegroups.com/article/view/10.21037/jtd-2024-2144/dss

Peer Review File: Available at https://jtd.amegroups.com/article/view/10.21037/jtd-2024-2144/prf

Conflicts of Interest: All authors have completed the ICMJE uniform disclosure form (available at https://jtd.amegroups.com/article/view/10.21037/jtd-2024-2144/coif). The authors have no conflicts of interest to declare.

Ethical Statement: The authors are accountable for all aspects of the work in ensuring that questions related to the accuracy or integrity of any part of the work are appropriately investigated and resolved. The study was conducted in accordance with the Declaration of Helsinki (as revised in 2013) and was approved by the Ethics Committee of The First Affiliated Hospital of Guangzhou Medical University (Nos. 2018-82 and ES-2024-K161-01). All patients provided their written informed consent.

References

1. Siegel RL, Giaquinto AN, Jemal A. Cancer statistics, 2024. CA Cancer J Clin 2024;74:12-49.
2. Ettinger DS, Wood DE, Aisner DL, et al. Non-Small Cell Lung Cancer, Version 3.2022, NCCN Clinical Practice Guidelines in Oncology. J Natl Compr Canc Netw 2022;20:497-530.
3. Yasuda H, Kobayashi S, Costa DB. EGFR exon 20 insertion mutations in non-small-cell lung cancer: preclinical data and clinical implications. Lancet Oncol 2012;13:e23-31.
4. Paez JG, Jänne PA, Lee JC, et al. EGFR mutations in lung cancer: correlation with clinical response to gefitinib therapy. Science 2004;304:1497-500.
5. Zhang L, Wang Y, Gao J, et al. Non coding RNA: A promising diagnostic biomarker and therapeutic target for esophageal squamous cell carcinoma (Review). Oncol Lett 2024;27:255.
6. Lynch TJ, Bell DW, Sordella R, et al. Activating mutations in the epidermal growth factor receptor underlying responsiveness of non-small-cell lung cancer to gefitinib. N Engl J Med 2004;350:2129-39.
7. Rosell R, Carcereny E, Gervais R, et al. Erlotinib versus standard chemotherapy as first-line treatment for European patients with advanced EGFR mutation-positive non-small-cell lung cancer (EURTAC): a multicentre, open-label, randomised phase 3 trial. Lancet Oncol 2012;13:239-46.
8. Osoegawa A, Karashima T, Takumi Y, et al. Osimertinib as first-line treatment for recurrent lung cancer patients with EGFR mutation. J Thorac Dis 2023;15:5566-73.
9. Moyer JD, Barbacci EG, Iwata KK, et al. Induction of apoptosis and cell cycle arrest by CP-358,774, an inhibitor of epidermal growth factor receptor tyrosine kinase. Cancer Res 1997;57:4838-48.
10. Li D, Ambrogio L, Shimamura T, et al. BIBW2992, an irreversible EGFR/HER2 inhibitor highly effective in preclinical lung cancer models. Oncogene 2008;27:4702-11.
11. Guo L, Zhou G, Huang M, et al. The impact of EGFR T790M mutation status following the development of Osimertinib resistance on the efficacy of Osimertinib in non-small cell lung cancer: A meta-analysis. Clin Respir J 2024;18:e13748.
12. Cross DA, Ashton SE, Ghiorghiu S, et al. AZD9291, an irreversible EGFR TKI, overcomes T790M-mediated resistance to EGFR inhibitors in lung cancer. Cancer Discov 2014;4:1046-61.
13. Yang JC, Ahn MJ, Kim DW, et al. Osimertinib in Pretreated T790M-Positive Advanced Non-Small-Cell Lung Cancer: AURA Study Phase II Extension Component. J Clin Oncol 2017;35:1288-96.
14. Lu K, Tse V, Altaie G, et al. Efficacy and tolerability of osimertinib with dabrafenib and trametinib in BRAF V600E acquired EGFR-mutant non-small cell lung cancer: a case series. J Thorac Dis 2024;16:5379-87.
15. Thress KS, Paweletz CP, Felip E, et al. Acquired EGFR C797S mutation mediates resistance to AZD9291 in non-small cell lung cancer harboring EGFR T790M. Nat Med 2015;21:560-2.
16. Planchard D, Loriot Y, André F, et al. EGFR-independent

mechanisms of acquired resistance to AZD9291 in EGFR T790M-positive NSCLC patients. Ann Oncol 2015;26:2073-8.
17. Ou SI, Agarwal N, Ali SM. High MET amplification level as a resistance mechanism to osimertinib (AZD9291) in a patient that symptomatically responded to crizotinib treatment post-osimertinib progression. Lung Cancer 2016;98:59-61.
18. Shi P, Oh YT, Zhang G, et al. Met gene amplification and protein hyperactivation is a mechanism of resistance to both first and third generation EGFR inhibitors in lung cancer treatment. Cancer Lett 2016;380:494-504.
19. Ortiz-Cuaran S, Scheffler M, Plenker D, et al. Heterogeneous Mechanisms of Primary and Acquired Resistance to Third-Generation EGFR Inhibitors. Clin Cancer Res 2016;22:4837-47.
20. Kim TM, Song A, Kim DW, et al. Mechanisms of Acquired Resistance to AZD9291: A Mutation-Selective, Irreversible EGFR Inhibitor. J Thorac Oncol 2015;10:1736-44.
21. Jassem J, Dziadziuszko R. Nazartinib in EGFR Thr790Met-mutant non-small-cell lung cancer. Lancet Respir Med 2020;8:528-9.
22. Ham JS, Kim S, Kim HK, et al. Two Cases of Small Cell Lung Cancer Transformation from EGFR Mutant Adenocarcinoma During AZD9291 Treatment. J Thorac Oncol 2016;11:e1-4.
23. White JC, Pucci P, Crea F. The role of histone lysine demethylases in cancer cells' resistance to tyrosine kinase inhibitors. Cancer Drug Resist 2019;2:326-34.
24. Jarry U, Bostoën M, Pineau R, et al. Orthotopic model of lung cancer: isolation of bone micro-metastases after tumor escape from Osimertinib treatment. BMC Cancer 2021;21:530.
25. Ohe Y, Imamura F, Nogami N, et al. Osimertinib versus standard-of-care EGFR-TKI as first-line treatment for EGFRm advanced NSCLC: FLAURA Japanese subset. Jpn J Clin Oncol 2019;49:29-36.
26. Capel B, Swain A, Nicolis S, et al. Circular transcripts of the testis-determining gene Sry in adult mouse testis. Cell 1993;73:1019-30.
27. Hansen TB, Jensen TI, Clausen BH, et al. Natural RNA circles function as efficient microRNA sponges. Nature 2013;495:384-8.
28. Conn VM, Chinnaiyan AM, Conn SJ. Circular RNA in cancer. Nat Rev Cancer 2024;24:597-613.
29. Xu J, Ji L, Liang Y, et al. CircRNA-SORE mediates sorafenib resistance in hepatocellular carcinoma by stabilizing YBX1. Signal Transduct Target Ther 2020;5:298.
30. Li X, Yang L, Chen LL. The Biogenesis, Functions, and Challenges of Circular RNAs. Mol Cell 2018;71:428-42.
31. Wang C, Tan S, Liu WR, et al. RNA-Seq profiling of circular RNA in human lung adenocarcinoma and squamous cell carcinoma. Mol Cancer 2019;18:134.
32. Tao F, Gu C, Li N, et al. New biomarker for lung cancer - focus on circSETD3. J Biol Regul Homeost Agents 2021;35:583-91.
33. Chu J, Fang X, Sun Z, et al. Non-Coding RNAs Regulate the Resistance to Anti-EGFR Therapy in Colorectal Cancer. Front Oncol 2021;11:801319.
34. Zhang D, Yang Y, Kang Y, et al. Dysregulated expression of microRNA involved in resistance to osimertinib in EGFR mutant non-small cell lung cancer cells. J Thorac Dis 2023;15:1978-93.
35. Li K, Peng ZY, Wang R, et al. Enhancement of TKI sensitivity in lung adenocarcinoma through m6A-dependent translational repression of Wnt signaling by circ-FBXW7. Mol Cancer 2023;22:103.
36. Gao GB, Chen L, Pan JF, et al. LncRNA RGMB-AS1 inhibits HMOX1 ubiquitination and NAA10 activation to induce ferroptosis in non-small cell lung cancer. Cancer Lett 2024;590:216826.
37. Lin Z, Feng F, Liang J, et al. lncRNA RP11-10A14.5: a potential prognosis biomarker for LUAD through regulation on proliferation and metastasis. Discov Oncol 2022;13:32.
38. Kim D, Langmead B, Salzberg SL. HISAT: a fast spliced aligner with low memory requirements. Nat Methods 2015;12:357-60.
39. Li H, Handsaker B, Wysoker A, et al. The Sequence Alignment/Map format and SAMtools. Bioinformatics 2009;25:2078-9.
40. Liao Y, Smyth GK, Shi W. featureCounts: an efficient general purpose program for assigning sequence reads to genomic features. Bioinformatics 2014;30:923-30.
41. Memczak S, Jens M, Elefsinioti A, et al. Circular RNAs are a large class of animal RNAs with regulatory potency. Nature 2013;495:333-8.
42. Lau KW, Zeng H, Liang H, et al. Bioinformatics-based identification of differentiated expressed microRNA in esophageal squamous cell carcinoma. Transl Cancer Res 2018;7:1366-75.
43. Li J, Chen Y, Shi X, et al. A systematic and genome-wide correlation meta-analysis of PD-L1 expression and targetable NSCLC driver genes. J Thorac Dis 2017;9:2560-71.
44. Kobayashi S, Boggon TJ, Dayaram T, et al. EGFR mutation and resistance of non-small-cell lung cancer to gefitinib. N Engl J Med 2005;352:786-92.

45. Kobayashi S, Ji H, Yuza Y, et al. An alternative inhibitor overcomes resistance caused by a mutation of the epidermal growth factor receptor. Cancer Res 2005;65:7096-101.
46. Sun Q, Lei X, Yang X. CircRNAs as upstream regulators of miRNA//HMGA2 axis in human cancer. Pharmacol Ther 2024;263:108711.
47. Wei L, Sun J, Zhang N, et al. Novel Implications of MicroRNAs, Long Non-coding RNAs and Circular RNAs in Drug Resistance of Esophageal Cancer. Front Cell Dev Biol 2021;9:764313.
48. Li B, Zhu L, Lu C, et al. circNDUFB2 inhibits non-small cell lung cancer progression via destabilizing IGF2BPs and activating anti-tumor immunity. Nat Commun 2021;12:295.
49. Peng W, He D, Shan B, et al. LINC81507 act as a competing endogenous RNA of miR-199b-5p to facilitate NSCLC proliferation and metastasis via regulating the CAV1/STAT3 pathway. Cell Death Dis 2019;10:533.
50. Chen T, Yang Z, Liu C, et al. Circ_0078767 suppresses non-small-cell lung cancer by protecting RASSF1A expression via sponging miR-330-3p. Cell Prolif 2019;52:e12548.
51. Zhao J, Li L, Wang Q, et al. CircRNA Expression Profile in Early-Stage Lung Adenocarcinoma Patients. Cell Physiol Biochem 2017;44:2138-46.
52. Luo YH, Yang YP, Chien CS, et al. Plasma Level of Circular RNA hsa_circ_0000190 Correlates with Tumor Progression and Poor Treatment Response in Advanced Lung Cancers. Cancers (Basel) 2020;12:1740.
53. Wei C, Peng D, Jing B, et al. A novel protein SPECC1-415aa encoded by N6-methyladenosine modified circSPECC1 regulates the sensitivity of glioblastoma to TMZ. Cell Mol Biol Lett 2024;29:127.
54. Guo Z, Chen Y, Wu Y, et al. CircRNA regulates the liquid-liquid phase separation of ATG4B, a novel strategy to inhibit cancer metastasis? Cell Stress 2024;8:56-8.
55. Yang J, Qi F, Tan B, et al. circSPECC1 promotes bladder cancer progression via regulating miR-136-5p/GNAS axis. Pathol Res Pract 2022;234:153914.
56. Lim SM, Syn NL, Cho BC, et al. Acquired resistance to EGFR targeted therapy in non-small cell lung cancer: Mechanisms and therapeutic strategies. Cancer Treat Rev 2018;65:1-10.
57. Bersanelli M, Minari R, Bordi P, et al. L718Q Mutation as New Mechanism of Acquired Resistance to AZD9291 in EGFR-Mutated NSCLC. J Thorac Oncol 2016;11:e121-3.
58. Assadollahi V, Rashidieh B, Alasvand M, et al. Interaction and molecular dynamics simulation study of Osimertinib (AstraZeneca 9291) anticancer drug with the EGFR kinase domain in native protein and mutated L844V and C797S. J Cell Biochem 2019;120:13046-55.
59. Niederst MJ, Hu H, Mulvey HE, et al. The Allelic Context of the C797S Mutation Acquired upon Treatment with Third-Generation EGFR Inhibitors Impacts Sensitivity to Subsequent Treatment Strategies. Clin Cancer Res 2015;21:3924-33.
60. Wang S, Song Y, Yan F, et al. Mechanisms of resistance to third-generation EGFR tyrosine kinase inhibitors. Front Med 2016;10:383-8.
61. Matsumura T, Nakamura-Ishizu A, Takaoka K, et al. TUBB1 dysfunction in inherited thrombocytopenia causes genome instability. Br J Haematol 2019;185:888-902.
62. Bolton-Gillespie E, Schemionek M, Klein HU, et al. Genomic instability may originate from imatinib-refractory chronic myeloid leukemia stem cells. Blood 2013;121:4175-83.
63. Jiao Q, Bi L, Ren Y, et al. Advances in studies of tyrosine kinase inhibitors and their acquired resistance. Mol Cancer 2018;17:36.
64. Wu HM, Shao LJ, Jiang ZF, et al. Gemcitabine-Induced Autophagy Protects Human Lung Cancer Cells from Apoptotic Death. Lung 2016;194:959-66.
65. Subbiah V, Kreitman RJ, Wainberg ZA, et al. Dabrafenib plus trametinib in patients with BRAF V600E-mutant anaplastic thyroid cancer: updated analysis from the phase II ROAR basket study. Ann Oncol 2022;33:406-15.
66. Nagasaka M, Balmanoukian AS, Madison R, et al. Amivantamab (JNJ-61186372) induces clinical, biochemical, molecular, and radiographic response in a treatment-refractory NSCLC patient harboring amplified triple EGFR mutations (L858R/ T790M/G796S) in cis. Lung Cancer 2022;164:52-5.
67. Kristensen LS, Hansen TB, Venø MT, et al. Circular RNAs in cancer: opportunities and challenges in the field. Oncogene 2018;37:555-65.

(English Language Editor: J. Gray)

Cite this article as: Hao Z, Feng F, Wang Q, Wang Y, Li J, Huang J. Circular RNA *SPECC1* promoted tumorigenesis and osimertinib resistance in lung adenocarcinoma via a circular RNA-microRNA network. J Thorac Dis 2024;16(12):8754-8770. doi: 10.21037/jtd-2024-2144